Ionic diffusion in voltage-clamped isolated cardiac myocytes
Implications for Na,K-pump studies

David J. Mogul,* Donald H. Singer,‡§ and Robert E. Ten Eick§
The Departments of *Electrical Engineering and Computer Science, ‡Medicine (Reingold ECG Center, Division of Cardiology), and §Pharmacology, Northwestern University, Chicago, Illinois 60611

ABSTRACT The whole-cell voltage-clamp technique employing electrolyte-filled micro-pipette suction electrodes is widely used to investigate questions requiring an electrophysiological approach. With this technique, the ionic composition of the cytosol is assumed to be strongly influenced (as result of diffusion) by the ionic composition of the solution contained in the electrode. If this assumption is valid for isolated cardiac myocytes, the technique would be particularly powerful for studying the dependence of their Na,K-pump on the intracellular [Na^+]. However, the relationship between the concentrations of ions in the solution filling the electrode and those in the cytosol has not been established. The relationship was investigated to determine in particular whether the [Na^+] at the intracellular cation ligand binding sites for the Na-pump ($[Na^+]_{ps}$) can be set and clamped by [Na^+] in the pipette electrode ($[Na^+]_{pip}$). If $[Na^+]_{pip}$ can set and clamp $[Na^+]_{ps}$, this would provide a means for defining the dependence of the Na,K-pump on intracellular [Na^+]. The relationship between $[Na^+]_{pip}$ and $[Na^+]_{ps}$ was analyzed using two approaches. First, a mathematical model of three-dimensional ionic diffusion within a whole-cell patch-clamped myocyte was developed and the effects of experimental parameters on mean $[Na^+]_{ps}$ were investigated. When typical experimental values were simulated, the time course to achieve steady state mean $[Na^+]_{ps}$ was found to be most sensitive to variations in electrode pore size, cell length and the Na^+ pumping rate, but at steady state, mean $[Na^+]_{ps}$ varies from $[Na^+]_{pip}$ by 5% or less depending on pump rate. Second, to provide experimental support for the validity of the simulations, isolated ventricular myocytes were voltage-clamped and the reversal potential for the Na current was determined in order to estimate steady state intracellular [Na^+]. The results of the mathematical and experimental analyses suggest that steady state $[Na^+]_{ps}$ can be regulated by the [Na^+] in suction pipette electrodes. These findings, while also having a broader significance, indicate for isolated cardiac myocytes that whole-cell suction micro-electrodes can provide a means to assess the dependence of the Na,K-pump on $[Na^+]_{ps}$.

INTRODUCTION

The rate of cellular Na^+ extrusion by the cardiac Na,K-pump is regulated, in part, by the Na^+ concentration at the intracellular sarcolemmal pump sites involved with binding Na^+ ($[Na^+]_{ps}$). However, a precise quantitative description of the relationship between pump rate and $[Na^+]_{ps}$ for intact cardiac cells has not been established because of ambiguity in the interpretation of the relationship between $[Na^+]_{ps}$ and estimates of intracellular Na^+ activity (a_i^{Na}) obtained during typical kinetic studies of the Na,K-pump using ion-selective electrodes (ISE) in conjunction with Na-loading techniques (e.g., Thomas, 1972; Eisner et al., 1981*a*; Wasserstrom et al., 1983; Sejersted et al., 1987). Depletion of $[Na^+]_{ps}$ relative to the average a_i^{Na} might develop during generation of a large pump current. Thus, if intracellular concentration gradients occur, or if, during Na,K-pump mediated recovery from an intracellular Na^+-load the Na^+ level changes significantly faster than the equilibration time for these electrodes, a_i^{Na} as sensed by ISE may not accurately reflect $[Na^+]_{ps}$. In addition, because cytosolic ionic concentrations are not controlled during recovery from a Na^+-load, the elevated but rapidly diminishing a_i^{Na} is expected to alter continuously both the rates of the Na^+:H^+ and Na^+:Ca^{++} exchangers and the passive Na^+ leak. This would affect a_i^{Na} in ways that have been attributed solely to the Na,K-pump thereby confounding any assessment of the Na^+ dependence of the Na,K-pump. Therefore, the advantage of fixing or "clamping" $[Na^+]_{ps}$ at known levels during experiments designed to assess the effect of the $[Na^+]_{ps}$ on Na,K-pumping is clear.

The whole-cell voltage-clamp technique employing electrolyte-filled suction micro-pipettes appears to offer a powerful alternative approach for investigating the intracellular Na dependence of the Na,K-pump because, in addition to permitting pump current to be measured, it provides an opportunity to modify the intracellular [Na^+]. Ideally, $[Na^+]_{ps}$ should be effectively "clamped"

Address correspondence to David J. Mogul, Ph.D., Department of Pharmacological and Physiological Sciences, University of Chicago, 947 East 58 Street, Chicago, IL 60637.

by the Na^+ concentration of the solution filling wide-tipped electrodes thus permitting a quantitative steady state analysis of the Na^+ sensitivity of pump function. However, this approach should not be regarded as providing data adequate for a reliable analysis until the relationship between the Na^+ concentration in the solution filling the micro-pipette electrode ($[Na^+]_{pip}$) and $[Na^+]_{ps}$ is established and the degree of control of $[Na^+]_{ps}$ by the pipette solution is determined. This report presents the results of a theoretical and experimental investigation of this relationship. It was defined during voltage clamp at −40 mV so that any voltage dependence of the pump current could be neglected and passive voltage-dependent inward Na^+ leak would be minimized. A rigorous three-dimensional mathematical analysis of intracellular ionic diffusion was employed to examine how several experimental parameters could affect the relationship between $[Na^+]_{pip}$ and $[Na^+]_{ps}$ during whole-cell experiments. Analyses of intracellular diffusion have been published previously (for example: Safford and Bassingthwaighte, 1977; Fischmeister and Horackova, 1983; Chang, 1985; Simon and Llinas, 1985; Oliva et al., 1988). However, the earlier approaches could not be adapted for this study because they assumed certain geometrical conditions and symmetries that cannot be regarded as valid for the more complex whole-cell patch-clamp situation. Therefore, we developed a new and unique model.

In addition to findings based on simulations using the mathematical model which demonstrate the feasibility of using the whole-cell patch pipette to control intracellular ion concentrations, we also present experimental evidence, which appears to confirm the validity and utility of the model and supports the notion that a Na^+ concentration clamp is possible during experiments designed to study the Na,K-pump in isolated cardiac cells using the whole-cell voltage-clamp technique, provided certain experimental conditions are maintained. This was accomplished using the whole-cell voltage-clamp technique to monitor the Na current reversal potential (V_{Na}) as an index of the equilibrium (Nernst) potential for Na^+ (E_{Na}) in isolated cardiac myocytes; the value and limitations of such measurements are discussed. Thus use of the whole-cell voltage-clamp technique to quantitatively assay the intracellular Na^+ dependence of the Na,K-pump in intact cells appears to be feasible, and the findings should have broad application to investigations of other intracellular ion-dependent processes.

SIMULATION METHODS

Model system

Diffusion analysis was performed in the cylindrical coordinate system in order to model the pertinent myocyte geometry. A schematic diagram of the system is shown in Fig. 1. An impermeant high resistance seal between the glass microelectrode and the cell membrane is assumed. Access between microelectrode and cytosol is obtained when the membrane patch beneath the microelectrode pore is broken. The microelectrode is centered in the middle of the myocyte, and p_o represents the pore diameter of the microelectrode and r_o and l_o the radius and length of the cell, respectively. Unlike most other diffusion models in the current literature, neither radial nor longitudinal symmetry were assumed. Only symmetry across the vertical plane ABCD shown in Fig. 1 and the plane perpendicular to ABCD centered in the middle of the myocyte (which would cut the cell and electrode into left and right halves) was assumed.

Diffusion model

The diffusion of a substance with concentration, U, in the nonsteady state can be described by a parabolic partial differential equation:

$$\frac{\partial U}{\partial t} = D\nabla^2 U, \tag{1}$$

where D is the appropriate diffusion coefficient and ∇ is the Laplacian operator in the relevant coordinate system and dimension. Since it is the effect on $[Na^+]_{ps}$ of cations diffusing out of the microelectrode that is of interest, and because the area of access of the microelectrode to the intracellular space is only a small fraction of the total membrane surface area, symmetry is limited to the two planes mentioned previously.

Therefore, a closed-form solution is not possible, and description of the diffusion process in all three spatial dimensions is required:

$$\frac{\partial U}{\partial t} = D\left[\frac{\partial^2 U}{\partial r^2} + \frac{1}{r}\frac{\partial U}{\partial r} + \frac{1}{r^2}\frac{\partial^2 U}{\partial \theta^2} + \frac{\partial^2 U}{\partial z^2}\right], \tag{2}$$

where r, θ, and z are the radial, angular, and longitudinal coordinates. For simplicity, isotropic diffusion was assumed.

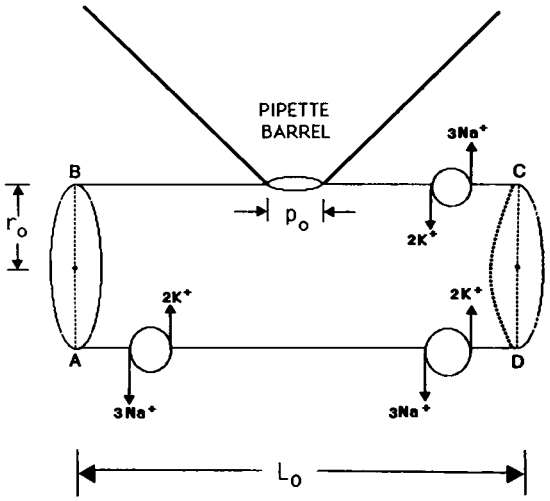

FIGURE 1 Schematic of suction pipette voltage clamp system as it was modeled. Access to myocyte cytosol by the microelectrode is obtained when membrane patch underneath electrode pore is broken. p_o represents pore diameter. r_o and l_o are the radius and length of cell, respectively. Efflux of a Na^+ load occurs through the Na,K-pump with a 3:2 Na^+:K^+ stoichiometry.

Boundary conditions

The source of cations at the interface between microelectrode and cell was assumed to be a reservoir having an infinite capacity such that:

$$U(\theta, z, r_o, t) = [Na^+]_{pip}$$

$$(t \geq 0; |\theta| < \theta_p; z \leq p_o), \quad (3)$$

where $\theta_p = \sin^{-1}(p/2r_o)$. Concentrations rather than activities are used throughout this paper to simplify the analysis. To solve for the boundary conditions at every location on the cell membrane where a Na,K-pump site exists, it was necessary to assume that the microelectrode solution represents an infinite reservoir of Na^+. Oliva et al. (1988), in a study that did not account for either any transmembrane ionic flux or the radial asymmetry of a patch-clamped myocyte, recently analyzed the effect of pipette geometry on ionic diffusion. Their findings, which are thus restricted to the electrode side of the electrode-cell interface, suggest that when flux rates to and out of the electrode pore are large, an electrode barrel-to-tip concentration gradient can develop. However, this gradient disappears as cellular $[Na^+]$ approaches and equals $[Na^+]_{pip}$. For the sake of simplicity, the extent to which the steady state flux of Na^+ occurring during active Na^+-pumping will result in a barrel-to-tip gradient has not been accounted for in our model. If one is primarily concerned with the time-course of achieving steady state cellular $[Na^+]$, clearly this gradient cannot be ignored. However, since our study is concerned primarily with the level of the steady state cellular $[Na^+]$, the gradient associated with a nonequilibrium state would be of little or no consequence. As will be indicated subsequently, the simulated steady state cellular $[Na^+]$ and the experimentally-estimated levels are virtually identical, indicating that it is acceptable to define the steady state $[Na^+]$ at the pore-cell interface equal to $[Na^+]_{pip}$. Therefore, the simulations by Oliva et al. (1988) complement those of this study, having impact only on the time course of reaching steady state $[Na^+]_{ps}$ and not on its level.

In modeling the Na,K-pump flux at each of 256 evenly distributed pump sites (J_{pump}), Na^+ influx occurring via passive leak is assumed to be balanced by the steady state Na^+ efflux due to the pump. However, when $[Na^+]_{ps}$ increases beyond this equilibrium value, pump flux will increase proportionally to the additional Na^+ load (Cohen et al., 1984; Rasmussen et al., 1986). Thus:

$$J_{pump} = k\,(U - U_{equil}) \quad (4)$$

$$k = 3\,I_{pump}/\{F\,(U - U_{equil})\}, \quad (5)$$

where $U = [Na^+]_{ps}$, U_{equil} is the equilibrium $[Na^+]_{ps}$ at which passive influx equals active efflux, I_{pump} is the pump current density attributable to a Na^+ load, F is Faraday's constant, and the Na,K pump ratio is assumed to be 3:2. This formulation accounts for both passive Na influx and active Na efflux. Experimental data from Eisner et al. (1981*a*; Fig. 4 *B*) was used to solve for the net Na efflux rate constant, k, in Eq. 5. By definition, Eq. 5 describes a linear dependence of pump rate on $[Na^+]_{ps}$. While the results of Eisner et al. (1981*a*) imply that this dependence is linear, in fact the range of intracellular Na^+ concentration that they tested was narrow, not exceeding ~25 mM (assuming an intracellular Na activity coefficient of 0.75). Since any nonlinear characteristic of this relationship may not have been apparent due to the consequences of limited diffusion of activator cation in restricted extracellular spaces (Rasmussen et al., 1986), and because pump saturation may occur at an intracellular Na^+ much higher than 25 mM, the model presented here also includes a formulation for k in which a first-order Michaelis-Menten dependence on $[Na^+]_{ps}$ is assumed.

The boundary conditions for each of the 256 pump sites is:

$$-D \cdot \nabla U = J_{pump} \quad (6)$$

because the rate at which Na^+ reaches the surface must equal the rate at which Na^+ leaves the surface. Diffusion at the internal cell-surface is assumed to occur normal to that surface. Elsewhere on the surface (except at the electrode interface):

$$-D \cdot \nabla U = 0. \quad (7)$$

In our simulations, $D = 5 \times 10^{-6}$ cm^2/s. While the diffusion of Na^+ in aqueous solution is faster, this value is consistent with the slower intracellular diffusion coefficient for Na^+ reported for frog semitendinous muscle (Kushmeric and Podolsky, 1969) and frog sartorius muscle (Ling, 1978).

The algorithm used to obtain a numerical solution to Eq. 2 was the alternating-direction implicit (ADI) method (Peaceman and Rachford, 1955; Gerald, 1980). The ADI technique takes advantage of the tri-diagonal matrix structure of this problem and solves the equation by alternating which dimension is calculated implicitly per time step. Time was advanced by 0.2 ms for each step. Results were consistent with simulations run using a smaller time step. Solution to the set of equations was derived using Gaussian elimination.

EXPERIMENTAL METHODS

Preparation of myocytes

Isolated guinea pig ventricular myocytes were prepared using a modification of the method described by Mitra and Morad (1985). Adult guinea pigs (250–300 gm) of either sex were sacrificed by cervical dislocation. The chest cavity was quickly exposed and the aorta was cannulated *in situ*. The heart was then excised, hung on a 0.75 m-high Langendorff column, and perfused at constant pressure through the aorta and coronary arteries retrogradely. The perfusate column was jacketed and a recirculating octanol-paraffin oil mixture was perfused through the jacket via a heat exchanger to maintain solution temperatures at 36°C. Two high intensity incandescent lamps were used to maintain the heart surface at a warm temperature during the perfusion.

The solutions used for cell isolation were vigorously bubbled with 100% O_2. For the first five minutes nominally Ca^{++}-free Tyrode's solution (in mM: NaCl, 135; KCl, 5.4; $MgCl_2$, 1; NaH_2PO_4, 0.33 Hepes, 10) was perfused through the heart to remove residual blood. The heart was then perfused to weaken the intercellular connective tissue by recirculating 25 ml of enzyme solution (Ca^+-free Tyrode's plus, in mg %: collagenase Type I, 150; Protease Type XIV, 20.6; [Sigma Chemical Co., St. Louis, MO] Albumin, 100) for 7.5 min. Finally, 100 ml of KB solution (in mM: KCl, 25; Hepes, 10; KOH, 115.9; glutamate, 80; taurine, 10; oxalic acid, 14; KH_2PO_4, 10; glucose, 11; EGTA, 0.5; with albumin, 100 mg %) replaced the enzyme-containing solution and the first 50 ml of the circulating KB solution were discarded.

The heart was then cut down from the perfusion apparatus and placed in the final 50 ml of KB solution. Approximately the apical half of the left and right ventricles were excised, minced with scissors (to help disperse the cells), and filtered through a 210 μm nylon mesh to harvest dispersed cells. The harvested cells were centrifuged gently for 15–20 s, the supernatant aspirated, and the pellet resuspended in the final solution. Only rod-shaped quiescent cells with clear, evenly-spaced striations were used.

Voltage clamp technique

Suction pipettes were made from borosilicate glass capillary tubes (1.1 mm i.d.; Garner Glass Co., Claremont, CA) using a vertical puller (Narishige Co., Japan). Current recordings were filtered with a low-

pass 11.4 kHz single-pole filter, sampled at 10 kHz, and recorded digitally using a PDP 11/73 (Digital Equipment Corp., Maynard, MA).

Inverted voltage-clamp pulses were applied to the bath through an Ag-AgCl pellet—KCl agar bridge. The voltage of the internal solution-filled micro-pipette suction electrodes was nulled with respect to ground potential with the pipette tips submerged in internal solution. Total series resistance produced by the pipette tip and cell interior was compensated for (typically ~65%) before recording membrane current by feeding back a fraction of the original signal into the command pulse. Uncompensated series resistances were 0.8 ± 0.3 MΩ. The maximal currents elicited during determination of V_{Na} for I_{Na} never exceeded ~1.5 nA. Therefore, the maximal voltage errors should be <2 mV. Experiments were performed at 31°C (±1°C).

Experimental solutions

The internal solution contained (mM): Na-Glutamate, 50; CsCl, 110; Hepes (*N*-2-hydroxyethylpiperazine-*N'*-2-ethanesulfonic acid), 5; EGTA (ethyleneglycol-bis-(beta-aminoethylether)*N,N,N',N'*-tetra-acetic acid), 10; MgATP, 2; pH, 7.2 at 22°C. The external solution consisted of (mM): KCl, 5.4; $CaCl_2$, 1.8; $MgCl_2$, 1.2; $BaCl_2$, 0.5; $CdCl_2$, 1.0; CsCl, 5; Hepes, 5.5; glucose, 11.1; TMA-Cl + NaCl, 143; pH, 7.4 at 22°C.

MODELING RESULTS

The simulated steady state $[Na^+]_{ps}$ and the time course of mean $[Na^+]_{ps}$ to reach steady state (derived from the sum of the currents produced by each of the simulated pump sites) were plotted rather than $[Na^+]_{ps}$ of the individual sites because the whole-cell voltage-clamp technique yields membrane current that is summed over the entire membrane surface (i.e., whole-cell current). In all the simulations, $[Na^+]_{pip}$ exceeds equilibrium $[Na^+]_{ps}$. All simulations were run using the conditions listed below unless stated otherwise in the figure legends:

$$[Na^+]_{pip} = 50 \text{ mM}$$

$$\text{equilibrium } [Na^+]_{ps} = \text{initial } [Na^+]_i = 10 \text{ mM}$$

$$D = 0.5 \times 10^{-5} \text{ cm}^2/\text{s}$$

$$l_o = 100 \ \mu\text{m}$$

$$r_o = 10 \ \mu\text{m},$$

the extracellular K^+-binding pump site remains fully saturated and, a nonsaturating pump dependence on $[Na^+]_{ps}$.

Values reported for pipette pore diameter, p_o, in voltage clamp experiments vary (e.g., 4–5 μm, Gadsby et al., 1985; 10–15 μm, Brown et al., 1981). Simulations were run with p_o = 6.38 μm except when p_o was varied to examine the effect of electrode size on mean $[Na^+]_{ps}$. An equilibrium $[Na^+]_{ps}$ of 10 mM corresponds to the typical resting $[Na^+]_i$ when $[K^+]_o$ is ~ 5 mM. In these simulations it is assumed that intracellular Ca^{++} and H^+ are well-buffered. It is also assumed that inward Ca^{++} current (I_{Ca}) and the inward-rectifying K^+ current (I_{K1}) are blocked. In addition, membrane potential is assumed to be clamped at a level that both minimizes and fixes the voltage-dependent Na^+ flux (i.e., −40 mV). These conditions are equivalent to those typically used to investigate the Na,K-pump experimentally (Gadsby et al., 1985).

Effect of Na pumping on mean $[Na^+]_{ps}$

To investigate whether active Na^+ extrusion affects mean $[Na^+]_{ps}$, simulations were run with various values for the pump rate constant, k (Fig. 2). A constant pore size (p_o = 6.38 μm) was assumed. At k = 0, the Na,K-pump is modeled as if completely inhibited. Mean $[Na^+]_{ps}$ begins to rise as soon as electrode access to the cytosol is obtained (t = 0) and reaches steady state equal to $[Na^+]_{pip}$, as expected for a closed cylinder. Normal cellular pump rate is defined as $k = 1 \times 10^{-6}$ cm/s. At this value, the rate of rise of mean $[Na^+]_{ps}$ is nearly the same as in the case of zero pump-function. However, the steady state level as defined by mean $[Na^+]_{ps}$ at the end of 90 s is less than that for k = 0 by ~0.9 mM (i.e., ~2%). When pump rate is set at double the standard rate ($k = 2 \times 10^{-6}$), the rate of rise of mean $[Na^+]_{ps}$ is unchanged from that of the previous examples and steady state level is again slightly diminished from that of zero pump-function, in this case by ~1.8 mM. Using the standard pump rate, the difference in intracellular $[Na^+]$ directly under the electrode pore compared to $[Na^+]$ at the same depth at the end of the cell is 62% at three seconds of simulated time but drops to a difference of 10.3%, 2.5%, or 1.9% at the end of 30, 60, or 90 s, respectively.

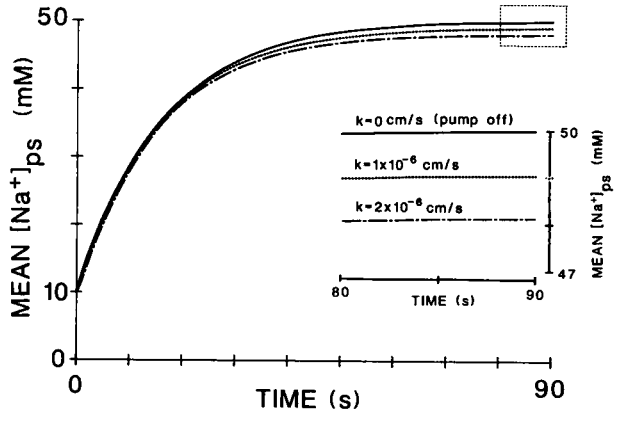

FIGURE 2 The effect of three different simulated Na,K-pump rates (k) on mean Na^+ concentration at the pump sites. Microelectrode access to myocyte cytosol is obtained at t = 0. $[Na^+]_{pip}$ = 50 mM. The insert shows the last ten seconds simulated, plotted in expanded scale.

Saturating versus non-saturating dependence of Na,K-pump on mean $[Na^+]_{ps}$

In both cases of active Na extrusion just shown, the pump rate was assumed to be linearly dependent on $[Na^+]_{ps}$ at each of the individual pump sites. The effect of a saturating dependence of the Na,K-pump on Na^+, however, may alter the kinetics and steady state level of mean $[Na^+]_{ps}$ if intracellular Na^+ increases to, or exceeds the half-maximal activation value ($K_{0.5}$) for Na^+-activation of the pump. Estimates for $K_{0.5}$ in red blood cells (Sachs, 1970), squid giant axon (Kracke and DeWeer, 1982), and sheep cardiac Purkinje strands (Fozzard et al., 1986) place K_D between 10 and 30 mM $[Na^+]_i$. A saturable dependence on Na^+ was modeled by modifying k to exhibit first order rate kinetics in which $K_{0.5}$ was estimated to be 20 mM. This value has been used as an estimated lower limit to explain the large differences reported for K-affinity of the Na,K-pump (Cohen et al., 1984).

Fig. 3 compares simulations when the previously cited two nonzero pump rate constants possess either saturating or nonsaturating ($K_{0.5} = \infty$) kinetics. Rate of rise of mean $[Na^+]_{ps}$ is unaffected by any of the formulations for k. However, when $k = 1 \times 10^{-6}$, steady state mean $[Na^+]_{ps}$ for the saturating model is ~0.25 mM closer to $[Na^+]_{pip}$. When $k = 2 \times 10^{-6}$, the steady state $[Na^+]_{ps}$ again deviates from $[Na^+]_{pip}$ less for the saturating model than for the nonsaturating model, the steady state difference in $[Na^+]_{ps}$ between the two models being ~0.5 mM. This difference will, of course, be dependent upon $[Na^+]_{pip}$ which, in this case, is 2.5 times $K_{0.5}$. Furthermore, as $K_{0.5}$ increases, steady state mean $[Na^+]_{ps}$ approaches that of the nonsaturating case.

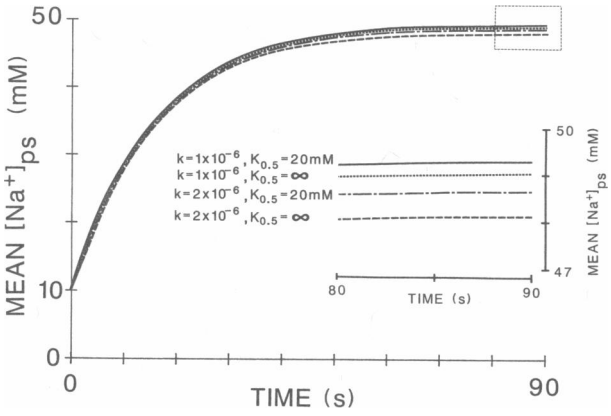

FIGURE 3 The effect of Na,K-pumping on mean $[Na^+]_{ps}$ when pump dependence on Na^+ obeys first order saturable rate kinetics with a $K_{0.5}$ of 20 mM vs. a pump with nonsaturable ($K_{0.5} = \infty$) kinetics. Two values of k are simulated. (*Insert*) last 10 s in expanded scale.

As a test of whether $[Na^+]_{ps}$ can be set and controlled by the $[Na^+]_{pip}$, the effects of a saturating ($K_{0.5} = 20$ mM) v.s. nonsaturating Na^+ dependence of the pump on the mean $[Na^+]_{ps}$ at steady state were compared at various concentrations of Na^+ in the pipette. The results are plotted in Fig. 4. The line of identity (slope = 1) represents a system in which the micro-pipette electrode can perfectly control mean $[Na^+]_{ps}$ at steady state. Deviation of mean $[Na^+]_{ps}$ from this line was most evident at $[Na^+]_{pip}$ = 100 mM although this deviation did not exceed 2.2% of $[Na^+]_{pip}$ regardless of pump formulation. Differences in simulation results between the two pump models decreased as $[Na^+]_{pip}$ decreased since the effects of saturation are less prominent as Na^+ approaches or falls below $K_{0.5}$.

Effect of myocyte length on mean $[Na^+]_{ps}$

Because the physical dimensions of myocytes may vary, the influence of myocyte length on mean $[Na^+]_{ps}$ was examined. Cellular radius was maintained at 10 μm. Fig. 5 shows the results of using the standard rate constant for an active pump function in cells with lengths of 100 μm and 150 μm. The rate of rise of mean $[Na^+]_{ps}$ is slower for the longer cell. True steady state is still not achieved at 90 s. Although a difference of ~0.3 mM still exists at the end of the simulation, mean $[Na^+]_{ps}$ for the longer cell continues to approach the level for the shorter cell. It is apparent from these results that nonsteady state measurements should exhibit greater sensitivity to variations in cellular size than will steady state measurements. Thus

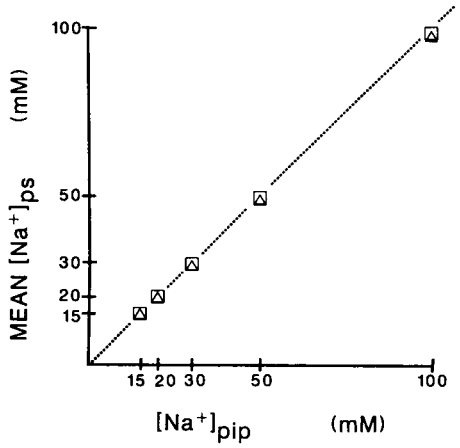

FIGURE 4 Mean $[Na^+]_{ps}$ calculated at steady state with different pipette Na^+ concentrations. Na,K-pump rate is at the standard value ($k = 1 \times 10^{-6}$ cm/s). Comparison of myocytes with linear nonsaturating Na,*K*-pump (triangles) vs. saturating Na,K-pump with $K_{0.5}$ = 20 mM (*squares*). Line of identity represented by the dashed line.

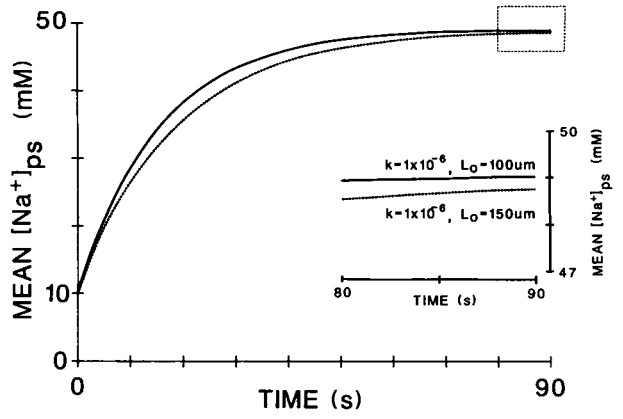

FIGURE 5 Time course of mean $[Na^+]_{ps}$ in two myocytes with different lengths. Na,K-pumping is at the standard rate for both cells as defined in the text. Cell radius is 10 μm. (*Insert*) last 10 s in expanded scale.

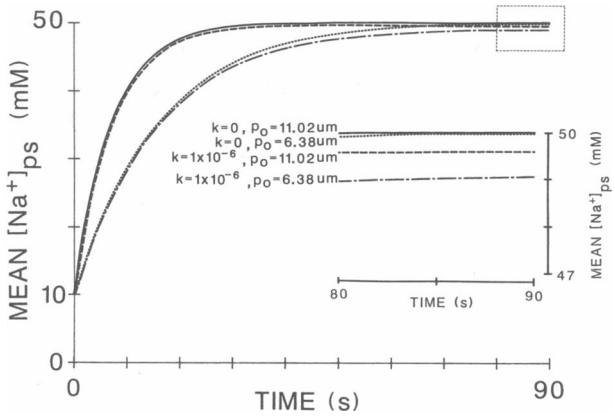

FIGURE 6 Effect of two different microelectrode pore diameters (p_o) on the time course of mean $[Na^+]_{ps}$. Two different pump rates are simulated. (*Insert*) last 10 s in expanded scale.

cell length is not expected to alter the ability of the pipette to clamp the steady state $[Na^+]_{ps}$ appreciably.

Effect of electrode pore size on mean $[Na^+]_{ps}$

Micropipette pore size can vary between voltage-clamp experiments due to differences in experimental technique as well as differences in electrode fabrication methods. Furthermore, upon rupture of the membrane patch beneath the pipette tip, residual membrane may partially obstruct access of the electrode solution to the cytosol. Therefore, although use of the term "pore size" implies unimpeded access between the internal pipette solution and the cytosol, it is in fact intended to mean only the actual area of solution interface between micropipette and myocyte.

The effect of different electrode pore sizes on diffusion of Na^+ is shown in Fig. 6. Two pore diameters are compared: 6.38 μm and 11.06 μm. Also, two Na,K-pump rate constants were used: $k = 0$ (pump off) and $k = 1 \times 10^{-6}$ (standard pump rate). When the pump is off, mean $[Na^+]_{ps}$ at steady state equals $[Na^+]_{pip}$ regardless of pore size which again confirms the result expected for a closed cylinder. The rate of rise of mean $[Na^+]_{ps}$ is very sensitive to pore size but shows little sensitivity to pump rate as shown earlier in Fig. 2. Although true steady state is not completely reached at 90 s, it is evident that decreasing the pore size increases the discrepancy in steady state mean $[Na^+]_{ps}$ for a given pump rate. With an active pump, at 90 s mean $[Na^+]_{ps}$ for the large pore exceeds that for the medium pore by ~0.52 mM. Steady state is achieved with an active pump and the smaller electrode in ~102 s (not shown). The effect of pore size on steady state $[Na^+]_{ps}$ will vary inversely with the pore area and thus with the square-root of the pore diameter. Thus, for example, if a pore diameter of 3.19 μm and a normal pump rate were simulated, the difference between $[Na^+]_{pip}$ and steady state $[Na^+]_{ps}$ is expected to be fourfold greater than when pore size is 6.38 μm. It also follows from the results shown in Figs. 3 and 6 that the effect of pore size on the difference between $[Na^+]_{pip}$ and steady state $[Na^+]_{ps}$ is expected to be amplified linearly by increasing pump rate (see Fig. 3). However, as will be seen subsequently, it is possible to use pipettes which, even in the face of the large Na^+-pump current expected when $[Na^+]_{pip}$ is 50 mM, will allow the steady state intracellular $[Na^+]$ to closely approximate $[Na^+]_{pip}$.

Binding of cations to phospholipids

The question of whether competitive binding of Na^+ and other cations to negatively-charged phospholipids could reduce steady state $[Na^+]_{ps}$ and thus change the apparent Na^+-dependence of the pump was examined. To accomplish this, the model was modified to reflect such reversible binding of cytosolic Na^+ by reducing its diffusion coefficient (Bassingthwaighte and Reuter, 1972; Safford and Bassingthwaighte, 1977; Simon and Llinas, 1985). The values used for the association constants for Na^+ (K_{Na}) and K^+ (K_K) binding to phospholipids were 0.6 and 0.15 M^{-1}, respectively (from Eisenberg et al., 1979). Membrane binding-site density, L, was assumed to be 1/70 A^{-2} (McLaughlin et al., 1979). Simulations revealed that both steady state $[Na^+]_{ps}$ and the rise-time of the time course to steady state were virtually insensitive to this type of Na^+ sequestration (results not shown). A likely explanation for the negligible effect of phospholipid binding is that, relative to the population of cations, the

density of these binding sites is very low. In addition, if one also simulates the effects of physiologically relevant concentrations of divalent cations, their binding further reduces the already minimal effect of monovalent cation binding.

EXPERIMENTAL RESULTS

Na^+ reversal potential

The reversal potential of the whole-cell-patch membrane current conducted by TTX-sensitive Na channels was monitored in voltage clamped guinea pig ventricular myocytes. Cd^{2+} and Ba^{2+} were added to the external solution to block I_{Ca} and I_{K1}, respectively, and Cs^+ was added to both internal and external solutions to limit permeability through K^+ channels. Na,K-pump activity was maintained by addition of Na^+ and Mg-ATP to the internal and K^+ to the external solutions. Fig. 7 shows the current-voltage (I-V) relationships when $[Na^+]_{pip}$ = 50 mM and two different concentrations of external Na^+ were applied at 31 ± 1°C. Assuming $[Na^+]_i$ equals $[Na^+]_{pip}$ at steady state, the Nernst potential (E_{Na}) should be −10 mV or +10 mV when $[Na^+]_o$ of 34.2 mM or 73.2 mM is used, respectively. If Na channels are permeable primarily to Na^+ and the independence principle were to apply, then the potential at which the Na current reverses should approximately equal E_{Na}.

Steady state V_{Na} was readily attained in myocytes bathed in either external Na^+ concentration tested. In these cases V_{Na} was within 1 mV of the predicted E_{Na} indicating that the intracellular $[Na^+]$ closely approximated $[Na^+]_{pip}$. This finding suggests that steady state $[Na^+]_{ps}$ is nearly equivalent to $[Na^+]_{pip}$. Results at steady state were consistent with predictions regardless of whether $[Na^+]_o$ was greater or less than $[Na^+]_{pip}$. Additional experiments (not shown, n = 6) performed at the same $[Na^+]_o$ display similar results with respect to steady state E_{Na}. However, the time course to achieving steady state varied by as much as a factor of four (3 to 12 min) between different voltage-clamped cells using different electrodes.

Varying $[Na^+]$ in the bath perfusion solution above and below $[Na^+]_{pip}$ should have revealed if there had been any significant sodium flux through a leaky seal between cell and electrode. This latter finding justifies the model's assumption that the electrode seal is impermeant to ions. Also, Donnan potentials between the pipette solution and cytosol, due to unequal mobilities of anions, apparently caused no detectable deviation of E_{Na}. It is possible that Donnan effects may have altered intracellular Na^+ and thus shifted E_{Na}. However, because this shift would be equally offset by an error in the measured membrane potential due to the Donnan potential, the effect of Donnan equilibrium on E_{Na} would be undetected. The error between true E_{Na} and the reversal potential for the Na current due to Donnan effects is expected to be small in any event because Donnan potentials measured in skinned skeletal (Godt and Baumgarten, 1984) and cardiac (Desilets and Baumgarten, 1986) muscle typically are < 5 mV.

DISCUSSION

The whole-cell voltage-clamp technique employing electrolyte-filled suction pipettes is widely used to investigate electrophysiological activity of many types of cells including cardiac myocytes. The ionic constituents of the solutions used to fill these wide-tipped electrodes are assumed to influence the cytosolic composition by passive diffusion although this assumption has not been rigorously tested. The goal of this study was to investigate this idea by simulating the diffusion of Na^+ from suction pipettes to the immediate vicinity of the intracellular sarcolemmal Na binding sites of the Na,K-pump. Specifically, we examined the question of whether the Na^+ concentration at the intracellular Na,K-pump sites can be defined and clamped at or near the Na^+ concentration in the pipette.

The simulations suggest that $[Na^+]_{ps}$ will reach a value very close to $[Na^+]_{pip}$ within several minutes under experimental conditions similar to those modeled. Therefore, if the experimental conditions are carefully chosen and $[Na^+]_{pip}$ is accurately known, it should be possible to define the relationship between $[Na^+]_{ps}$ and I_{pump} under steady state conditions with reasonable accuracy. Na current reversal potentials were determined during voltage clamp experiments performed under conditions similar to those modeled as a means to estimate intracellular $[Na^+]$ and to examine the usefulness of the model. The experimental results support the theoretical findings that the steady state $[Na^+]_{ps}$ can be both defined and well-controlled by $[Na^+]_{pip}$, if the experimental conditions are appropriate.

E_{Na} measurements

We have utilized an experimental method involving the Na channels to substantiate the results concerning $[Na^+]_{ps}$ that were derived by modeling. However, this approach for estimating the level of E_{Na} as the means to monitor $[Na^+]_{ps}$ does possess some limitations. Firstly, we have assumed that the Na current reversal potential accurately reflects E_{Na}. However, it is well-known that the TTX-sensitive Na channel is not exclusively permeant to Na^+ (Chandler and Meeves, 1965). If, for instance, channel permeability to Cs^+ is assumed to be 1% of that for Na^+, the apparent E_{Na} ($E_{Na'}$) measured using our

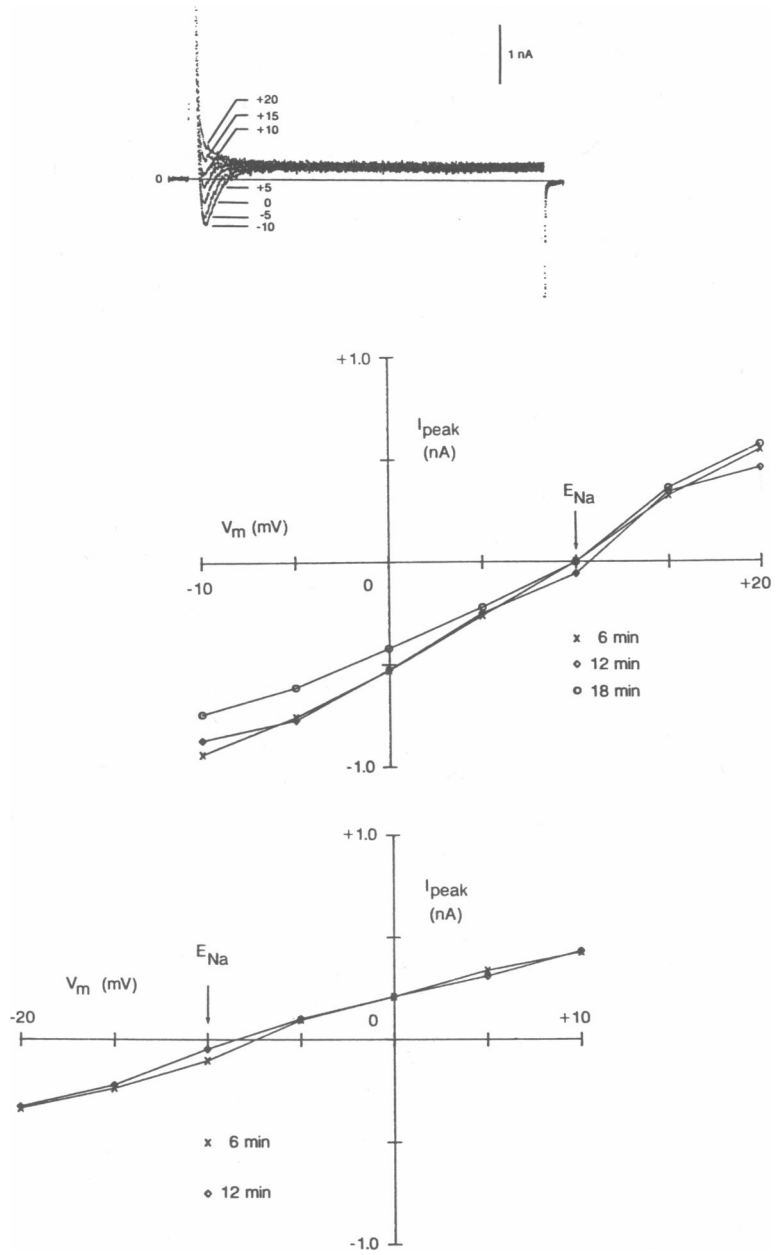

FIGURE 7 Experimental determination of reversal potential for the fast inward Na^+ channel. $[Na^+]_{pip}$ = 50 mM. T = 31°C. (*Upper trace*) Family of membrane currents from guinea pig ventricular myocytes recorded 6 min after access to the cytosol by electrode solution is obtained. $[Na^+]_o$ = 73.2 mM. Voltage clamp potentials shown. V_H = −40 mV. Pulse duration = 45 ms. (*Lower trace*) *I–V* relationships to show reversal potentials when $[Na^+]_o$ = 34.2 mM (*bottom*) and $[Na^+]_o$ = 73.2 mM (*top*) and holding potential = −40 mV. Current (I_{peak}) was measured as peak current minus the current at the end of a 45 ms pulse (i.e., steady state). Assuming $[Na^+]_i = [Na^+]_{pip}$, the predicted E_{Na} values are shown by arrows.

experimental solutions would be predicted to be positive to the true E_{Na} (+10 mV) by no more than ~0.08%. Therefore, we have assumed that the effect of other less permeant monovalent cations on E_{Na}, is negligible. Secondly, influx or efflux of Na^+ through Na channels, even if occurring only transiently, may alter the peri-membranal $[Na^+]$ as result of local intracellular accumulation or depletion. As a result, internal $[Na^+]$-dependent current may be modified. However, during clamp pulses used to define Na current reversal potential, inward Na^+ currents were small because pulsing was to potentials very close to E_{Na} and a 10 s interpulse interval should provide adequate

time to prevent significant pooling of Na^+ adjacent to the membrane. Therefore, the assumptions that these several effects can be regarded as negligible and that the experimentally derived value for intracellular $[Na^+]$ approximates the true intracellular $[Na^+]$ appear to be justifiable.

Steady state values of reversal potential observed when $[Na^+]_{pip}$ = 50 mM and $[Na^+]_o$ was varied are consistent with the modeling results at least to the degree of accuracy provided by the V_{Na} measurements. However, as noted earlier, there is a discrepancy between the time to reach steady state $[Na^+]_{ps}$ calculated from the model and that observed experimentally. Steady state E_{Na} was sometimes achieved two to four times more slowly than predicted by the model in some experiments. The most likely source of this discrepancy is the high sensitivity of the diffusion process to membrane pore size as shown in Fig. 6. Pipette access to the cytosol is obtained by membrane rupture. Partial obstruction of ion flow may occur when the membrane beneath the pipette pore is not completely removed. Thus estimates of pore diameter based on electrode resistance measurements taken in free solution are subject to variations during voltage clamp experiments. As shown by our model, the steady state level of $[Na^+]_{ps}$ is much less susceptible to variations in apparent pore size than is the kinetic time course to reach the steady state level. Thus, the experimental findings for the steady state are consistent with and appear to verify the simulation results.

Accounting for transmembrane Na^+ flux

The important source (or sink) for intracellular Na^+ influencing the outcome of suction pipette voltage-clamp experiments is the electrode solution that passively exchanges ions with the cytosol. Additional Na^+ influx which also may affect $[Na^+]_{ps}$ can occur through membrane channels and exchange mechanisms. Our model employs two assumptions concerning these transmembrane sources of Na^+. First, we have defined equilibrium for the system as the $[Na^+]_{ps}$ at which active Na efflux equals passive Na influx. This equilibrium value is assumed to be static and unchanging regardless of the extent to which $[Na^+]_{ps}$ is displaced from it by dialyzing the cytosol (with pipette solution). This is equivalent to postulating that Na influx is independent of $[Na^+]_i$ in a cell with an intact Na,K-pump capable of responding to a Na^+ load by increasing Na^+ transport. This assumption is reasonable because Gadsby (1980) showed in sheep Purkinje fibers that a 6-fold rise in $[Na^+]_i$ (from 5 mM to 30 mM) reduced passive Na^+ flux by <5%.

Secondly, the model assumes that Na,K-pump is the only significant route of Na^+ efflux. This assumption is expected to be most valid at modest levels of intracellular $[Na^+]$ (i.e., < 25 mM, Eisner et al., 1981*b*) because the time course of change of intracellular $[Na^+]$ and K^+-activated pump current are strongly correlated as noted by Cohen et al. (1984). This relationship has not been established for the higher levels of $[Na^+]_i$ that may be obtained when the Na/Ca and Na/H exchanges are brought into play during recovery from a proton or Ca^{++} load. Experimentally this situation can be avoided by appropriately buffering the internal solution with Hepes and EGTA or BAPTA (1,2-bis[o-aminophenoxy]ethane-*N*,*N*,*N'*,*N'*tetra-acetic acid). Therefore the simulations will reflect experimental results provided pH and pCa are controlled by the experimenter rather than by the Na^+-dependent cellular exchange mechanisms.

In order to test the effect of Na,K-pumping on the depletion of free-Na^+ around the pump sites we compared the results of simulations in which the pump was active to those in which the pump was inhibited. Pump inhibition was simulated by setting $k = 0$. Two effects need to be considered when pump activity is halted. First, experimentally-induced pump inhibition has been shown to produce an intracellular Na^+ load under certain conditions such that an intracellular accumulation of Na^+ above $[Na^+]_{pip}$ may occur. This situation has not been formally considered because many reports have been published showing that an intracellular Na^+ load can be pumped down to its equilibrium value upon Na,K-pump reactivation in cells in which Na^+ is not supplied by an extrinsic source such as an electrode. Therefore, only the effect of Na,K-pumping on depleting $[Na^+]_{ps}$ (relative to $[Na^+]_{pip}$) was examined because this depletion must exceed any accumulation effect on $[Na^+]_{ps}$ from a passive inward Na^+ leak.

Secondly, when the Na,K-pump is inhibited experimentally in a cell in which $[Na^+]_i$ is not clamped by an electrode as described above, steady state intracellular $[Na^+]$ rises as a consequence of an effect equivalent to an increase in the equilibrium $[Na^+]_i$ set-point. The value of this point is defined to be static in our model. However, the ability of a patch electrode to regulate $[Na^+]_{ps}$ is inversely proportional to the difference between $[Na^+]_{pip}$ and the equilibrium Na^+ point. Therefore, if the equilibrium $[Na^+]_i$ value increases for any reason, the capability of the electrode to control $[Na^+]_{ps}$ will be enhanced. Thus, our simulations are those of a "worst-case" situation.

Significance of experimental conditions to $[Na^+]_{ps}$

The effects on $[Na^+]_{ps}$ of selected experimental parameters that are particularly relevant to kinetic and steady state Na,K-pump studies were studied. The two parameters having the greatest effect in kinetic experiments in

which a continuously changing pump current is measured are the size of the myocyte and the pore diameter of the electrode. Fig. 3 shows that with an electrode resistance on the order of 1 MΩ (i.e., p_o = 6.38 μm), an increase in cell length results in a decrease in the rate of rise of mean $[Na^+]_{ps}$. The electrode pore diameter appears to be a major factor in determining both the rise time and steady state $[Na^+]_{ps}$ in voltage-clamp experiments. Of the parameters examined, pore diameter had the largest effect on $[Na^+]_{ps}$ rise time. However, there is a limit to what can be gained by increasing pore size. The technical difficulty of obtaining an adequate electrode-to-cell seal increases as pore diameter become more than a few percent of cell diameter. Such considerations require that the pore size of experimentally-used electrodes be a reasonable compromise which will minimize the resultant of several issues.

All five parameters studied exerted at least some influence on steady state mean $[Na^+]_{ps}$. However, even given the substantial difference between $[Na^+]_{pip}$ (50 mM) and the equilibrium concentration of Na^+ (10 mM), steady state mean $[Na^+]_{ps}$ was never less than $[Na^+]_{pip}$ by more than a few percent. The greatest discrepancy between the two values occurred when an active pump with linear dependence on Na^+ and a small pore diameter was considered. This indicates that steady state measurements should, in general, be much less sensitive than kinetic measurements to variations in any of the five experimental parameters tested. Fig. 4 is of particular significance to studies intended to characterize the dependence of some cellular or membrane process on the intracellular concentration of a substance that can be added to (or removed from) the solution used to fill micro-pipette suction electrodes. It suggests that, under standard simulation conditions (see results), the micro-pipette electrode can closely regulate mean steady state $[Na^+]_{ps}$ over a wide range of $[Na^+]_{pip}$.

Applicability of the model to other experimental paradigms

The characteristics of the model are importantly defined by the boundary conditions. Na^+ efflux is modeled strictly as a concentration dependent phenomenon. When a voltage-dependent ion channel or ion exchanger (e.g., Na:Ca exchange) are included, simulations of changes in membrane potential may require inclusion of nonlinearities in the boundary conditions that would greatly increase the complexity of the numerical solutions. For example, in the case of the Na,K-pump, variations in transmembrane potential may require modification of the pump parameter, k, in order to account for any significant degree of voltage dependence of the pump current (Gadsby et al., 1985; Nakao and Gadsby, 1986). Therefore, careful consideration of the experimental conditions is required for this model to be utilized correctly.

Diffusion is the rate-limiting step in the system we have modeled. That is, the diffusion of Na^+ from the microelectrode to the pump sites is the primary determinant of the quantity of ions that can offset depletion of these ions at the inner membrane surface. However, studies of time dependent fluxes of other substances may require a more complex analysis as the principal rate-limiting step may no longer be diffusion. An example is the sequestration of Ca^{2+} and its subsequent compartmentalization. The kinetics of simple diffusion may be modified by adding the effect of binding and unbinding (Crank, 1975; Safford and Bassingthwaighte, 1977; Fischmeister and Horackova, 1983) especially when these reactions have a complex concentration dependence (Fabiato and Fabiato, 1975; Allen and Kurihara, 1980).

SUMMARY

The Na,K-pump plays an important role in the maintenance of transmembrane ionic gradients. The suction pipette voltage clamp technique offers an opportunity to investigate the dependence of the Na,K-pump on intracellular Na^+. This paper presents an analysis that indicates that this technique can be employed to study further the Na^+-dependence of the Na,K-pump in voltage-clamped isolated cardiac myocytes; broader applications to other electrophysiological studies similarly using whole-cell suction-type micro-pipette electrodes as part of the experimental approach also seem feasible.

APPENDIX

Algorithms for solution to intracellular ionic diffusion

Three-dimensional ionic diffusion in the cylindrical coordinate system is described by Eq. A.1:

$$\partial U/\partial t = D[\partial U/\partial r^2 + r^{-1}\partial U/\partial r + r^{-2}\partial^2 U/\partial\theta^2 + \partial^2 U/\partial z^2]. \quad \text{(A.1)}$$

An analytical solution to the above equation is not available unless special symmetry conditions are assumed that are not valid to the experimental paradigm involving patch-clamped myocardial cells. Therefore, an alternate means of solving A.1 is required. The finite difference method provides a numerical technique for solution of the eigenvalues. Specifically, the alternating direction implicit (ADI) scheme was used in which each of the three coordinate axes is solved implicitly while the other two are solved explicitly per time step. Therefore, solution to equation A.1 occurred in three steps. Subscripts (i, j, k) represent positions on the three spatial axes (i.e., θ, z, r, respectively) and the superscripts represent positions in time. Each step has its own explicit approximation component and may be inherently

unstable such that unilateral repetition of a single step may lead to an unacceptable growth of errors. Therefore solutions are taken only after the third step in which the stability advantage of implicit calculations are maintained thereby containing errors within finite bounds so that the system remains stable overall. The following equations have omitted the diffusion coefficient, D, in order to simplify the already complicated notation. However, as stated in the text, the ionic diffusion rate was accounted for in the actual modeling.

Step 1 {θ implicit}

$$(U^{n+1}_{i,j,k} - U^{n}_{i,j,k})/\Delta t = r^{-2}[(U^{n+1}_{i+1,j,k} - 2U^{n+1}_{i,j,k} + U^{n+1}_{i-1,j,k})/(\Delta\theta)^2] + [(U^{n}_{i,j+1,k} - 2U^{n}_{i,j,k} + U^{n}_{i,j-1,k})/(\Delta z)^2] + [(U^{n}_{i,j,k+1} - 2U^{n}_{i,j,k} + U^{n}_{i,j,k-1})/(\Delta r)^2] + r^{-1}[(U^{n}_{i,j,k+1} - U^{n}_{i,j,k-1})/2\Delta r], \quad \text{(A.2)}$$

where $r = k \cdot \Delta r$.

Step 2 {z implicit}

$$(U^{n+2}_{i,j,k} - U^{n+1}_{i,j,k})/\Delta t = r^{-2}[(U^{n+1}_{i+1,j,k} - 2U^{n+1}_{i,j,k} + U^{n+1}_{i-1,j,k})/(\Delta\theta)^2] + [(U^{n+2}_{i,j+1,k} - 2U^{n+2}_{i,j,k} + U^{n+2}_{i,j-1,k})/(\Delta z)^2] + [(U^{n+1}_{i,j,k+1} - 2U^{n+1}_{i,j,k} + U^{n+1}_{i,j,k-1})/(\Delta r)^2] + r^{-1}[(U^{n+1}_{i,j,k+1} - U^{n+1}_{i,j,k-1})/2\Delta r]. \quad \text{(A.3)}$$

Step 3 {r implicit}

$$(U^{n+3}_{i,j,k} - U^{n+2}_{i,j,k})/\Delta t = r^{-2}[(U^{n+2}_{i+1,j,k} - 2U^{n+2}_{i,j,k} + U^{n+2}_{i-1,j,k})/(\Delta\theta)^2] + [(U^{n+2}_{i,j+1,k} - 2U^{n+2}_{i,j,k} + U^{n+2}_{i,j-1,k})/(\Delta z)^2] + [(U^{n+3}_{i,j,k+1} - 2U^{n+3}_{i,j,k} + U^{n+3}_{i,j,k-1})/(\Delta r)^2] + r^{-1}[(U^{n+3}_{i,j,k+1} - U^{n+3}_{i,j,k-1})/2\Delta r]. \quad \text{(A.4)}$$

Under these conditions the cell is insulated from its environment so that the boundary conditions may be expressed as:

$$\partial U/\partial r|_{j=r} = 0. \quad \text{(A.5)}$$

Eqs. A.2–A.5 may be expressed in matrix form:

$$AX = Y, \quad \text{(A.6)}$$

where A is the coefficient matrix, X is the vector of future values to be solved, and Y is the vector containing the coefficients of present values.

$$A = \begin{bmatrix} b & c & 0 & \cdot & \cdot & \cdot & A_{1,K} \\ a & b & c & & & & \cdot \\ 0 & a & b & c & & & \cdot \\ \cdot & & \cdot & \cdot & \cdot & & \cdot \\ \cdot & & & \cdot & \cdot & \cdot & \cdot \\ \cdot & & & & a & b & c \\ A_{K,1} & & \cdot & \cdot & \cdot & a & b \end{bmatrix}$$

so that a $(K \times K)$ tri-diagonal matrix is formed in which a, b, and c are the only nonzero elements and vary according to which step is being calculated implicitly. For step 1, these are:

$$a = c = -(\Delta\theta)^{-2} \quad b = (\Delta t^{-1} + 2(r\Delta\theta)^{-2}).$$

Taking the symmetry and the boundary condition of Eq. A.5 into account requires multiplication of elements $A_{1,2}$ and $A_{K,K-1}$ by 2. For step 2:

$$a = c = -(\Delta z)^{-2} \quad b = [\Delta t^{-1} + 2(\Delta z)^{-2}],$$

where $A_{1,2}$ and $A_{K,K-1}$ are also multiplied by 2 as above. For step 3:

$$a = -[\Delta r^{-2} - (r2\Delta r)^{-1}] \quad b = [\Delta t^{-1} + 2(\Delta r)^{-2}]$$
$$c = [\Delta r^{-2} + (r2\Delta r)^{-1}].$$

In the case of step 3, for $A_{1,1} = [\Delta t^{-1} + 2(r\Delta r)^{-1}]$, $A_{1,2} = -2(r\Delta r)^{-1}$ and $A_{K,K-1} = a$, as given above for this step.

The Y vectors can be calculated from known values.

For step 1:

$$Y_\lambda = \Delta z^{-2}U^{n}_{\lambda,j+1,k} + (\Delta t^{-1} - 2(\Delta z)^{-2} - 2(\Delta r)^{-2})U^{n}_{\lambda,j,k} + \Delta z^{-2}U^{n}_{\lambda,j-1,k} + (\Delta r^{-2} + (2r\Delta r)^{-1})U^{n}_{\lambda,j,k+1} + (\Delta r^{-2} - (2r\Delta r)^{-1})U^{n}_{\lambda,j,k-1}.$$

When $k = 1$, the above is altered by $(\Delta t^{-1} - 2(\Delta z)^{-2} - 2(2r\Delta r)^{-1})U^{n}_{\lambda,j,k}$ and $2(2r\Delta r)^{-1}U^{n}_{\lambda,j,k+1}$ to account for $\Delta r = r_0$ (the total radius of the cylinder as defined earlier.

For step 2:

$$Y_\lambda = (r\Delta\theta)^{-2}U^{n+1}_{i+1\lambda,k} + (\Delta t^{-1} - 2(r\Delta\theta)^{-2} - 2(\Delta r)^{-2})U^{n+1}_{i\lambda,k} + (r\Delta\theta)^{-2}U^{n+1}_{i-1\lambda,k} + (\Delta r^{-2} + (2r\Delta r)^{-1})U^{n+1}_{i\lambda,k+1} + (\Delta r^{-2} - (2r\Delta r)^{-1})U^{n+1}_{i,\lambda,j,k-1}.$$

When $k = 1$, the above is altered by $(\Delta t^{-1} - 2(r\Delta\theta)^{-2} - 2(2r\Delta r)^{-1})U^{n}_{i\lambda,k}$ and $2(2r\Delta r)^{-1}U^{n}_{i\lambda,k+1}$ to account for $\Delta r = r$ as in step 1.

For step 3:

$$Y_\lambda = (r\Delta\theta)^{-2}U^{n+2}_{i,j+1,\lambda} + (\Delta t^{-1} - 2(r\Delta\theta)^{-2} - 2(\Delta z)^{-2})U^{n+2}_{i,j,\lambda} + (r\Delta\theta)^{-2}U^{n+2}_{i-1,j,\lambda} + (\Delta z)^{-2}U^{n+2}_{i,j+1,\lambda} + (\Delta z)^{-2}U^{n+2}_{i,j-1,\lambda},$$

where $\lambda = 1 \ldots K$.

Vector X in Eq. A.6 was solved using Gaussian elimination. This nonpivoting elimination method with a tri-diagonal matrix is always stable, that is, with no growth of rounding errors. The technique also allows for efficient storage of intermediate values in computer memory.

Adjustments to equations to account for noninsulating boundary conditions. The cylindrical model as described by the above equations possesses closed boundaries. However, the goal is to model a single patch-clamped isolated myocyte. This requires taking into account open boundaries, namely transmembrane flux (see Eq. 6) and intracellular ionic diffusion with the solution in the microelectrode. Pump sites were located on the cylindrical surface but not at the ends since there is no evidence of significant Na,K-pumping at the tight junctions. Equations to describe these conditions were included in the model and can be accounted for by the following modifications.

I. Transmembrane flux

Five modifications to the model are required: (a) in matrix A of step 3: $A_{K,K} = k_{pump}[2(\Delta r)^{-1} + r^{-1}] + [\Delta t^{-1} + 2(\Delta r)^{-2}]$ (b) in matrix A of step 3: $A_{K,K-1} = -2(\Delta r)^{-2}$. The next three modifications are relevant when $r = r_o$ only (i.e., at the membrane surface) and are therefore applied only when $k = K$. (c) in the previously described vector Y of step 3: $Y_\lambda(\text{new}) = Y_\lambda(\text{old}) + k_{equil}(2\Delta r^{-1} + r^{-1})U_{equil}$ (d) in the previously described vector Y of step 1, the following modifications to the coeffi-

cients of U are made:

$$Y_\lambda = \cdots + \{k_{equil}(2\Delta r^{-1} + r^{-1}) + (\Delta t^{-1} - 2\Delta z^{-2} - 2\Delta r^{-2})\}U^n_{\lambda,j,k} + 2\Delta r^{-2}U^n_{\lambda,j,k-1} - k_{equil}(2\lambda r^{-1} + r^{-1})U_{equil}.$$

(e) In the previously described vector Y of step 2, the following modifications to the coefficients of U are made:

$$Y_\lambda = \cdots + \{k_{equil}(2\Delta r^{-1} + r^{-1}) + (\Delta t^{-1} - 2(r\Delta\theta^{-2} - 2\Delta r^{-2})\}U^{n+1}_{i,\lambda,k} + 2\Delta r^{-2}U^{n+1}_{i,\lambda,k-1} - k_{equil}(2\lambda r^{-1} + r^{-1})U_{equil}.$$

II. Ionic diffusion between pipette and myocyte

Four modifications are required to account for a large reservoir of Na^+ in the pipette in contact with the intracellular cytosol. These changes are made when integration is at the cell/pipette interface (that is, when $z <= p_o$ and $|\theta| < \theta_p$ as described in Simulation Methods). (a) matrix A in step 3 is altered during the above-mentioned conditions: $A_{K,K-1} = -[\Delta r^{-2} - (2r\Delta r)^{-1}]$; $A_{K,K} = \Delta t^{-1} + 2\Delta r^{-2}$ (b) vector Y in step 3 has the last (K) element changed: $Y_\lambda = [\Delta r^{-2} + (2r\Delta r)]U_{pip}$ where $U_{pip} = [Na^+]_{pip}$. The final two modifications have the additional criteria of occuring when $r = r_o$ (i.e., $k = K$): (c) vector Y in step 1: $Y_\lambda(new) = Y_\lambda(old) + (\Delta r^{-2} + (2r\Delta r)^{-1})U_{pip}$ (d) vector Y in step 2: $Y_\lambda(new) = Y_\lambda(old) + (\Delta r^{-2} + (2r\Delta r)^{-1})U_{pip}$.

The authors gratefully acknowledge helpful background discussions with Dr. Ira Cohen from the Department of Physiology and Biophysics, SUNY at Stonybrook, NY and with Dr. Helge Rasmussen from the Department of Cardiology, Royal North Shore Hospital, St. Leonard's, New South Wales, Australia.

Supported in part by Grants-in-Aid from the Reingold Estate, The Brinton Trust, The Cooley Trust, The Chicago Heart Association, and United States Public Health Service grant HL-27026.

REFERENCES

Allen, D. G., and S. Kuhira. 1980. Calcium transients in mammalian ventricular muscle. *Eur. Heart J.* 1:5–15.

Bassingthwaighte, J. B., and H. Reuter. 1972. Calcium movements and excitation-contraction coupling in cardiac cells. Electrical Phenomena in the Heart. W. C. DeMello, editor. Academic Press, Inc., New York. 353–395.

Brink, F. Jr. 1983. Linear range of Na^+ pump in sciatic nerve of frog. *Am. J. Physiol.* 244:C198–C204.

Brown, A. M., K. S. Lee, and T. Powell. 1981. Sodium current in single rat heart muscle cells. *J. Physiol. (Lond.).* 318:479–500.

Chandler, W. K., and H. Meves. 1965. Voltage clamp experiments on internally perfused giant axons. *J. Physiol. (Lond.).* 180:821–836.

Chang, D. C. 1985. Transport of Na^+ inside the giant axon of squid. *Cell Biophys.* 7:107–114.

Cohen, I., R. Falk, and G. Gintant. 1984. Saturation of the internal sodium site of the sodium pump can distort estimates of potassium affinity. *Biophys. J.* 46:719–727.

Cohen, J. A., and M. Cohen. 1981. Adsorption of monovalent and divalent cations by phospholipid membranes. *Biophys. J.* 36:623–651.

Crank, J. 1975. *The Mathematics of Diffusion.* Oxford University Press, London. 2nd ed.

Desilets, M., and C. M. Baumgarten. 1986. K^+, Na^+, and Cl^- activities in ventricular myocytes isolated from rabbit heart. *Am. J. Physiol.* 251:C197–C208.

Eisenberg, M., T. Gresalfi, T. Riccio, and S. McLaughlin. 1979. Adsorption of monovalent cations to bilayer membranes containing negative phospholipids. *Biochemistry.* 18(23):5213–5223.

Eisner, D. A., W. J. Lederer, and R. D. Vaughan-Jones. 1981*a*. The dependence of sodium pumping and tension on intracellular sodium activity in voltage-clamped sheep Purkinje fibres. *J. Physiol. (Lond.).* 317:163–187.

Eisner, D. A., W. J. Lederer, and R. D. Vaughan-Jones. 1981*b*. The effect of rubidium ions and membrane potential on the intracellular sodium activity of sheep Purkinje fibres. *J. Physiol. (Lond.).* 317:189–205.

Fabiato, A., and F. Fabiato. 1975. Contractions induced by a calcium-triggered release of calcium from the sarcoplasmic reticulum of single skinned cardiac cells. *J. Physiol. (Lond.).* 249:469–495.

Fischmeister, R., and M. Horackova. 1983. Variation of intracellular Ca^{2+} following Ca^{2+} current in heart: a theoretical study of ionic diffusion inside a cylindrical cell. *Biophys. J.* 41:341–348.

Fozzard, H. A., O. M. Sejersted, and J. A. Wasserstrom. 1986. Sodium activation of the Na,K-pump in isolated sheep cardiac Purkinje strands. *J. Physiol. (Lond.).* 381:91 P.

Gadsby, D. C., J. Kimura, and A. Noma. 1985. Voltage dependence of Na/K pump current in isolated heart cells. *Nature (Lond.).* 315:63–65.

Gadsby, D. 1980. Activation of electrogenic Na^+/K^+ exchange by extracellular K^+ in canine cardiac Purkinje fibers. *Proc. Natl. Acad. Sci. USA.* 77(7):4035–4039.

Gerald, C. F. 1980. Parabolic partial-differential equations. *In Applied Numerical Analysis.* C. F. Gerald, editor. Addison-Wesley, Reading, MA. pp. 390–432.

Glitsch, H. G., H. Pusch, and K. Venetz. 1976. Effects of Na and K ions on the active Na transport in guinea-pig auricles. *Pfluegers Arch. Eur. J. Physiol.* 365:29–36.

Godt, R. E., and C. M. Baumgarten. 1984. Potential and K^+ activity in skinned muscle fibers. *Biophys. J.* 45:375–384.

Kracke, G. R., and P. DeWeer. 1982. The rate coefficient of sodium efflux from squid giant axons. *Biophys. J.* 37:220a. (Abstr.)

Kushmeric, M. J., and R. J. Podolsky. 1969. Ionic mobility in muscle cells. *Science (Wash. DC).* 166:1297–1298.

Ling, G. 1978. Maintenance of low sodium and high potassium levels in resting muscle cells. *J. Physiol. (Lond.).* 280:105–123.

McLaughlin, S., N. Mulrine, T. Gresalfi, and A. McLaughlin. 1979. Adsorption of divalent cations to bilayer membranes containing phosphatidylserine. *J. Gen. Physiol.* 77:445–473.

Nakao, M., and D. Gadsby. 1986. Voltage dependence of Na translocation by the Na/K pump. *Nature (Lond.).* 323:628–630.

Peaceman, D. W., and H. H. Rachford. 1955. The numerical solution of parabolic and elliptic differential equations. *J. Soc. Ind. Appl. Math.* 3:28–41.

Oliva, C., I. S. Cohen, and R. T. Mathias. 1988. Calculation of time constants for intracellular diffusion in whole cell patch clamp configuration. *Biophys. J.* 54:791–799.

Rasmussen, H. H., D. J. Mogul, and R. E. TenEick. 1986. On the effect of unstirred layers on K^+ activated electrogenic Na^+ pumping in cardiac Purkinje strands. *Biophys. J.* 50:827–835.

Sachs, J. R. 1970. Sodium movement in the human red blood cell. *J. Gen. Physiol.* 56:322–341.

Safford, R. E., and J. B. Bassingthwaighte. 1977. Calcium diffusion in transient and steady states in muscle. *Biophys. J.* 20:113–136.

Simon, S. M., and R. R. Llinas. 1985. Compartmentalization of the sub-membrane calcium activity during calcium influx and its significance in transmitter release. *Biophys. J.* 48:485–498.

Thomas, R. C. 1972. Intracellular sodium activity and the sodium pump in snail neurones. *J. Physiol. (Lond.)*. 220:55–71.

Wasserstrom, J. A., D. J. Schwartz, and H. A. Fozzard. 1983. Relation between intracellular sodium and twitch tension in sheep cardiac Purkinje strands exposed to cardiac glycosides. *Circ. Res.* 53:697–705.